International Journal of Physical Sciences Vol. 7(12), pp. 1959 - 1966, 16 March, 2012
Available online at http://www.academicjournals.org/IJPS
DOI: 10.5897/IJPS12.059
ISSN 1992 - 1950 ©2012 Academic Journals

Full Length Research Paper

Implementation of edge detection algorithms to characterize magnetic micropillars patterned by X-ray lithography

U. Phromsuwan[1], C. Sirisathitkul[1], Y. Sirisathitkul[2]* and C. Sriphung[3]

[1]Magnet Laboratory, School of Science, Walailak University, Nakhon Si Thammarat, 80161, Thailand.
[2]School of Informatics, Walailak University, Nakhon Si Thammarat, 80161, Thailand.
[3]Synchrotron Light Research Institute, Nakhon Ratchasima, 30000, Thailand.

Accepted 28 February, 2012

The array of SU-8 photoresist pillars (10 × 10 × 50 μm) on a copper substrate was patterned by X-ray lithography using a synchrotron source. Flat cobalt films can then be sputter-deposited on the chemically stable and mechanically hardened SU-8 pillars in spite of geometry distortion and pattern collapse in some regions. Since any deviations from the pattern affect magnetic properties of the structure, images of these micropillars obtained from an optical microscope and a scanning electron microscope (SEM) were inspected using five different edge detection algorithms. The Canny and Laplacian of Gaussian (LoG) operators can detect all cross sections of micropillars, but noise points and lines were also included. The outputs from image processing by the Prewitt and Sobel operators yielded lower noise, but suffered from discontinuity, especially in the case of tilt angled SEM images. The Roberts cross edge detector had a weakest response to edges of the pattern under test. The 3D nature of the micropillars is an origin of low-contrast edge and background noise in the images.

Key words:X-ray lithography, SU-8 photoresist, high-aspect-ratio microstructure, image processing, edge detection.

INTRODUCTION

Micro and nanoscale magnetic patterns have been under investigations, because of their applications in recording, sensing and spintronic devices (Kikitsu et al., 2007; Terris, 2009). To fabricate such structures, a designate pattern is transferred onto a substrate by a lithography process using a masked irradiation on a layer of sensitive polymer resist. Among the variety of techniques, X-ray lithography offers some advantages, including a larger exposed area within a shorter time. X-rays are also able to penetrate a thick photoresist layer creating a high-aspect-ratio structure with vertical sidewalls (del Campo and Greiner, 2007; del Campo and Arzt, 2008). High-aspect-ratio pillars are desirable because stray fields from the magnetic deposits in the trenches do not interfere with those on the top (Kikitsu et al., 2007; Choi et al., 2010).

During the pattern transfer, the features can be deviated from the designate pattern. It follows that every lithographic structure contains errors in geometry and position. The inspection of repeated pattern is a tedious and time-consuming process. Computer programs are interesting alternatives for detecting objects and calculating relevant parameters such as area and volume distributions afterwards (Moropoulou et al., 2007; Yakar et al., 2010; Liu et al., 2011). In addition to circular and rectangular images, algorithms have been adapted to work in the case of objects with variations in shape (Marot and Bourennane, 2007; Zhang et al., 2011; Zhao, 2010). Despite successful trials in other fields including medical imaging (Smereka and Duleba, 2008; Sopharak

*Corresponding author. E-mail: syaowara@wu.ac.th. Tel: +66 75 672272. Fax: +66 75 672004.

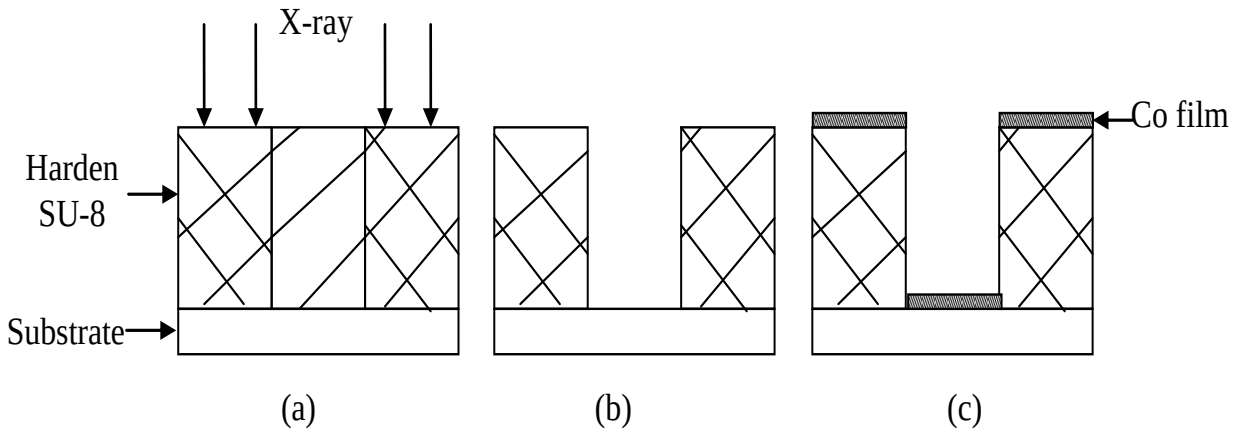

Figure 1. Process diagrams showing the structure after (a) X-ray exposure, (b) resist development and (c) magnetic deposition.

et al., 2009), the image processing is scarcely implemented in magnetic patterned structures (Nabavi et al., 2009). Several edge detection algorithms are potentially useful in such circumstance. In general, they track the intensity of 2D gray scale image and identify the direction whose intensity changes abruptly as the edge (Gonzalez et al., 2001). To compute the gradient of intensity as a function of the x and y coordinates, the Prewitt and the Sobel edge detector employ the 3×3 matrix as masks. The Prewitt operator is easier to implement, but the Sobel operator is superior in noise suppression. The center coefficient of the Sobel matrix is given more weight to promote the image smoothing. The Roberts Cross operator uses the 2×2 matrix to reduce a processing time, but the advantage from locating the center is absent. The Laplacian of Gaussian (LoG) operator incorporates a second derivative by using the Gaussian filter to smooth the image and the Laplacian filter to enhance edges. The Canny operator combines the smoothing and enhancement steps by convolving the image with a derivative of the Gaussian filter and determines the intensity discontinuities with a higher sensitivity making them also susceptible to noise.

In this work, arrays of SU-8 micropillars with an aspect ratio of 5 were patterned by X-ray lithography using the synchrotron radiation. The SU-8 photoresist, whose main components are Bisphenol A Novolak epoxy oligomer and triarylsulfonium hexafluoroantimonate salt, was chosen due to its high sensitivity to X-ray as well as excellent coating, processing and mechanical properties (del Campo and Greiner, 2007). In addition to usual photographing, micrographs of lithographic structures were assessed by image processing algorithms. The processes of pattern fabrication and image analysis are detailed in Materials and Methods. Micrographs of the obtained structures are presented and followed by results and discussion on the output from image processing using different edge detectors.

MATERIALS AND METHODS

A pattern of repeated 10×10 µm squares on a graphite mask with 10 µm spacing was transferred to substrates by an X-ray exposure. Pieces of copper spin-coated with a layer of 50 µm thick SU-8 were used as substrates. To remove the solvent and improve the adhesion between layers, the substrates were soft-baked at 95°C for 40 min and were dried at room temperature for 24 h before the exposure. In a masked irradiation, X-ray of wavelength 1.24 nm from the beam line BL6a of the Synchrotron Light Research Institute, Thailand was irradiated onto the substrate placed under the mask for 10 min. The exposed resist in an area about 5×5 mm was then left at room temperature for 24 h before developing.

The SU-8 patterned substrates were used in the radio frequency (RF) sputtering of cobalt. In the sputtering chamber with a cobalt target (99.95%) of 7.7 cm in diameter and 0.6 cm in thickness, argon gas of 51 sccm was employed as the operating gas during the film deposition. The cobalt film was grown on the patterned substrate using the RF power of 200 W for 3 min. The diagrams of the structure after the X-ray exposure, the resist development and the magnetic deposition are as shown in Figure 1. After the deposition, cobalt films on the arrays of SU-8 pillars were inspected by an optical microscope and a scanning electron microscopy (SEM).

SEM and optical micrographs of patterned pillars on the substrate were analyzed by an image processing program on MatLab. Functions are indicated by italic fonts in the diagram in Figure 2. In step 3, five different edge detection algorithms, namely (a) Canny, (b) LoG, (c) Prewitt, (d) Roberts Cross and (e) Sobel, were compared. As summarized in Figure 2, no threshold is applied and other default values are used for setting each edge detectors. The output of each edge detector composed of lines and points. Since the former may be from either micropattern or noise, a number of detected lines is also recorded and used as a performance indicator. Before applying these edge detectors to magnetic micropattern, they were tested with a hand-made image of an 11×6 array of circles to verify the comparison under a

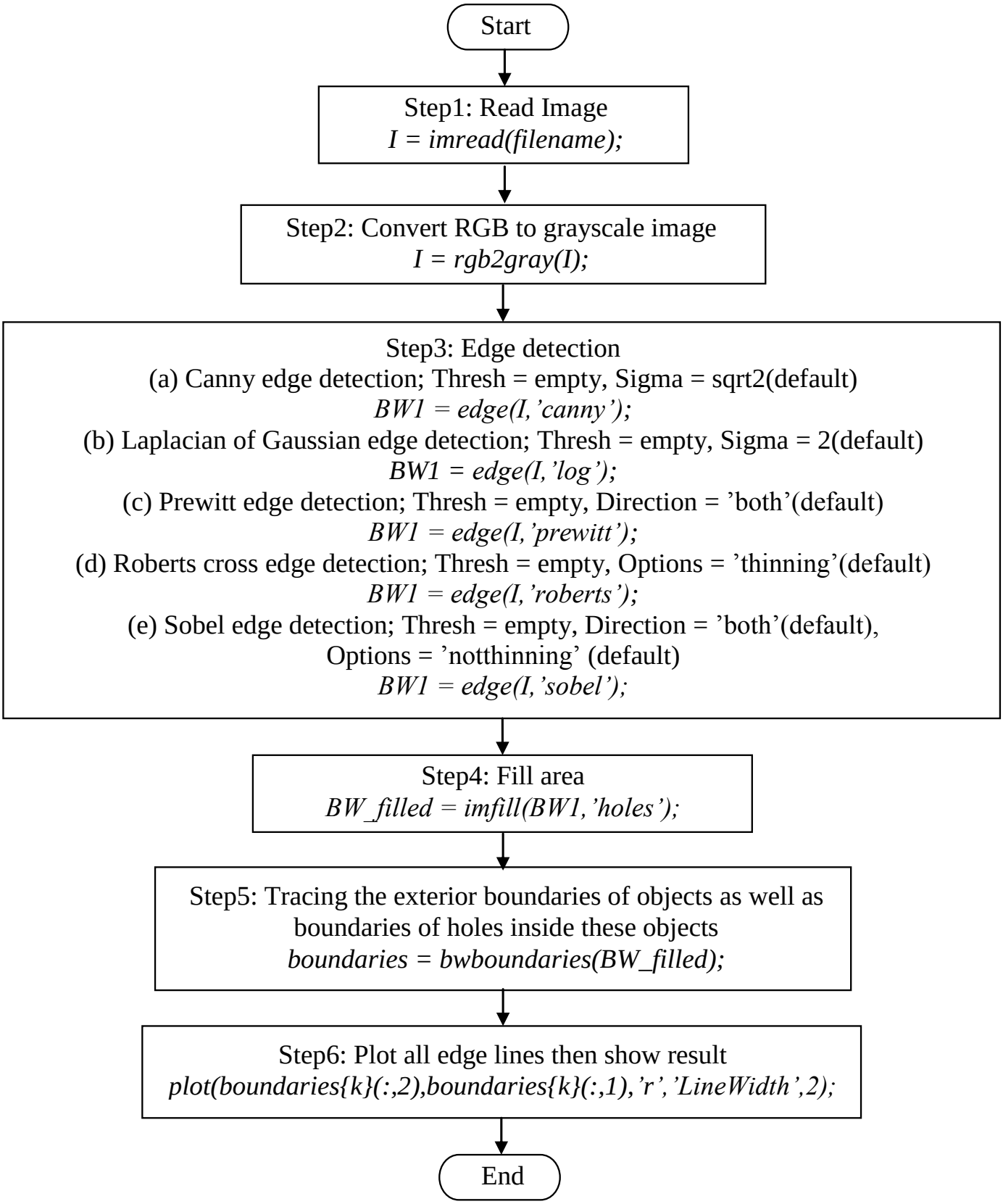

Figure 2. Diagrams showing the steps in the image processing program using five different edge detection algorithms.

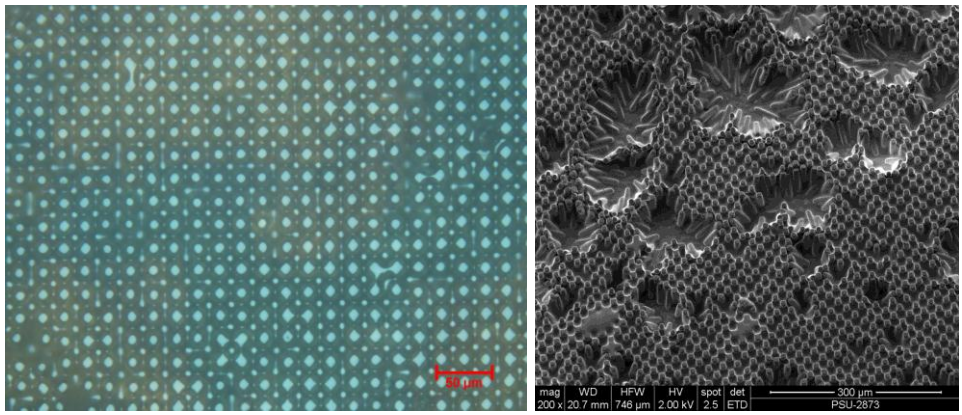

Figure 3. (a) Optical and (b) SEM micrographs of SU-8 arrays on a copper substrate.

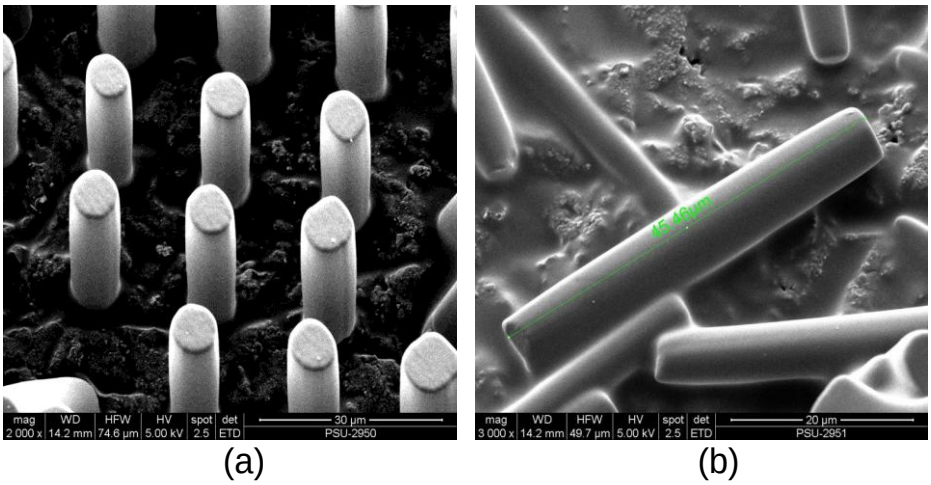

Figure 4. SEM micrographs of SU-8 pillars after cobalt deposition showing (a) patterned regions and (b) collapsed SU-8 pillars revealing their sidewalls and height.

circumstance with a limited number of lines and sharp boundary. Such image is referred to as a primitive image.

RESULTS AND DISCUSSION

Morphology of magnetic micropillars

By the process of masked irradiation, the physical and chemical properties of the SU-8 resist exposed to the X-ray are modified because triarylsulfonium hexafluoroantimonate salt decomposes and reacts with epoxy oligomer (del Campo and Greiner, 2007). Because the cross-linking in these exposed areas reduces the solubility to the developer, only the hardened parts of SU-8 remain on the copper substrate after developing, while the rest is washed away. From the top-view micrographs of the developed SU-8 pillars as shown in Figure 3(a), the cross sections appear as bright dots under the optical microscope with distortion in pattern geometry. These deviations in size and shape results from the imperfect mask irradiation and resist development. According to an SEM micrograph of the cobalt deposition on a patterned substrate in Figure 3(b), a pattern collapse occurs in certain regions where the adhesion between SU-8 resist and copper is weak. The capillary force in the developing and rinsing stages is a major factor in the detachment between the resist and the copper layer (del Campo and Greiner, 2007).

With a higher magnification, Figure 4(a) shows an example of a patterned region. Each pillar has some distortion in lateral dimensions from 10 × 10 µm. Their corners are curved resulting in irregular cross sections. Nevertheless, smooth cobalt films are observed implying

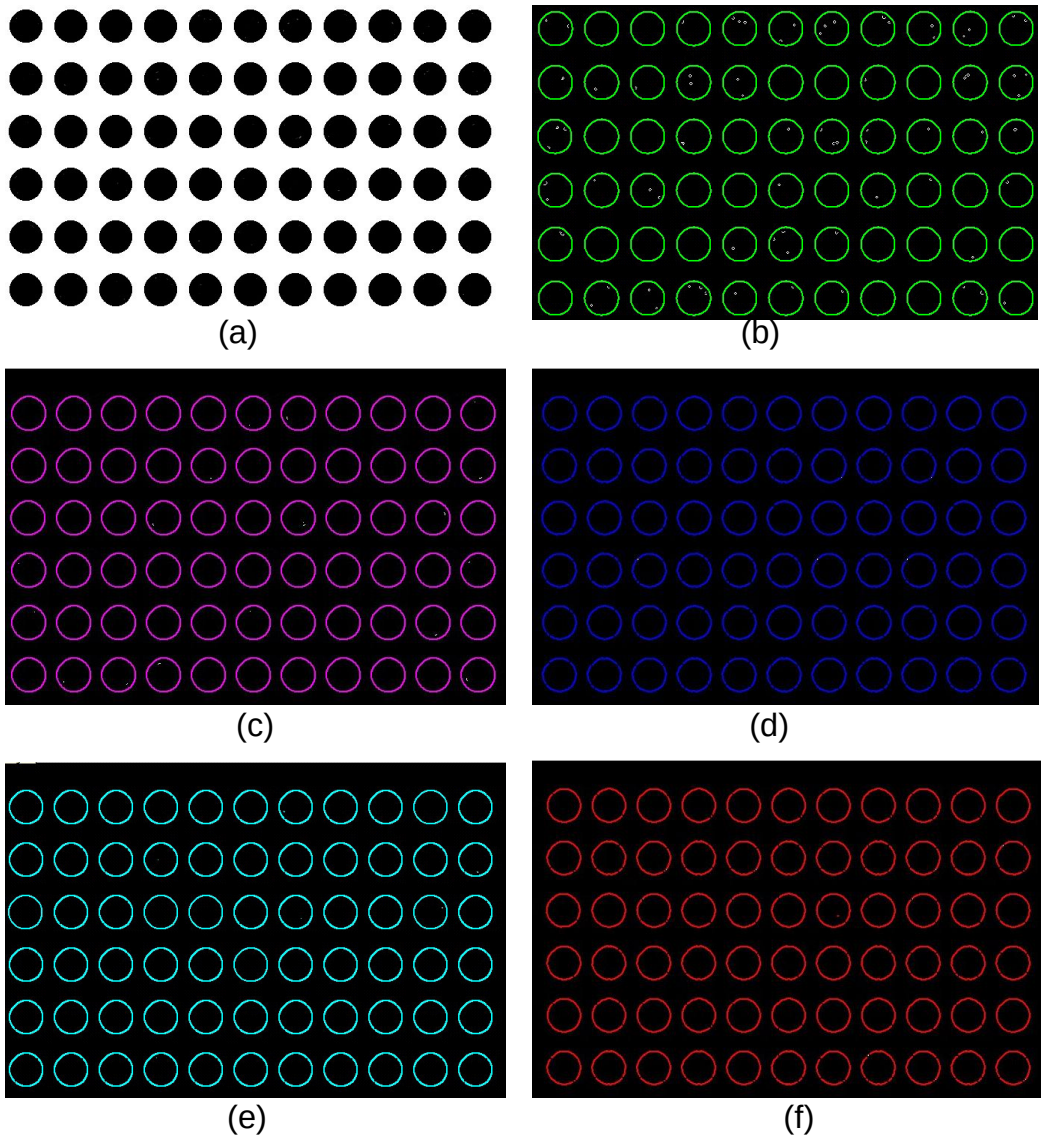

Figure 5. (a) Primitive image and its corresponding outputs from (b) Canny, (c) LoG, (d) Prewitt, (e) Roberts Cross and (f) Sobel operators.

that the SU-8 pillars possess small flatness errors. In a collapse region as shown in Figure 4b, the smooth vertical sidewalls of pillars are revealed without T-profiles meaning that the effects of diffraction and X-ray absorption are minimal (del Campo and Arzt, 2008). The height of each pillar can also be approximated as 45 µm.

Implementation of image processing

Every algorithm successfully detects all 66 circles in Figure 5a, but the difference in their performance is noticeable. It is noted that the outputs from Canny and LoG operators also exhibit small numbers of noise points because of their high sensitivity. In Table 1, the numbers of lines detected by both algorithms are precisely 66 accounting for 100%. The other three operators yield more than 100% suggesting that their outputs contain discontinuity which may not be evident from Figure 5d to f.

When all algorithms are implemented in the real optical micrograph as shown in Figure 6, even the Canny and LoG operators give rise to very different outputs. The output from the Canny operator seriously suffers from spurious detections from the background as shown in Figure 6b. The number of detected lines for 154 cross sections by all algorithms in Table 1 is beyond 1500, but

Table 1. Comparison of output from five edge detection algorithms in terms of the number of detected lines from micrographs and a primitive image.

Algorithm	Number of detected lines		
	Primitive image	Optical micrograph	SEM micrograph
Canny	66	3297	1252
LoG	66	2702	1096
Prewitt	233	1613	391
Roberts Cross	113	1840	483
Sobel	166	1567	397

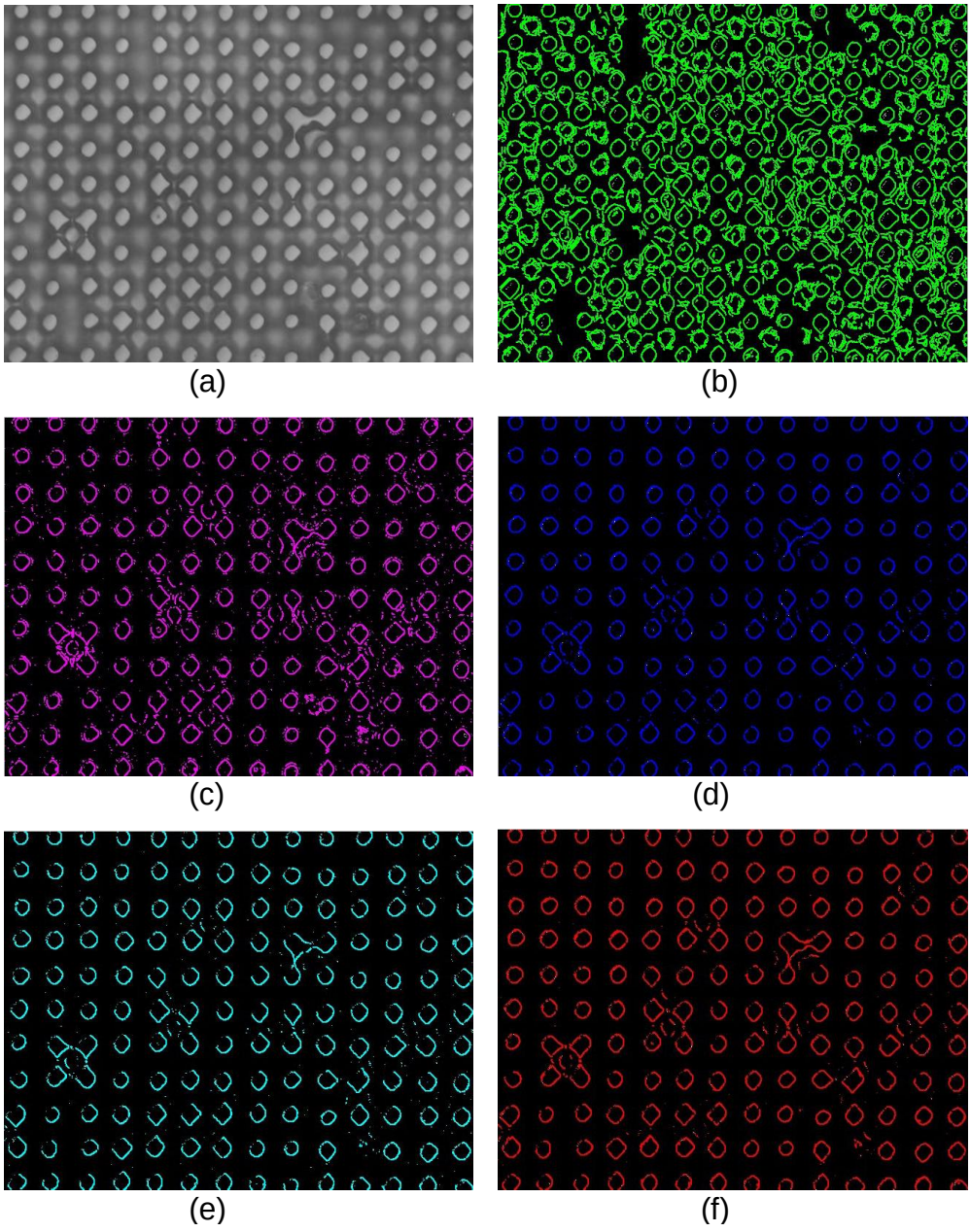

Figure 6. (a) Optical micrograph of SU-8 cross sections and its corresponding outputs from (b) Canny, (c) LoG, (d) Prewitt, (e) Roberts Cross and (f) Sobel operators.

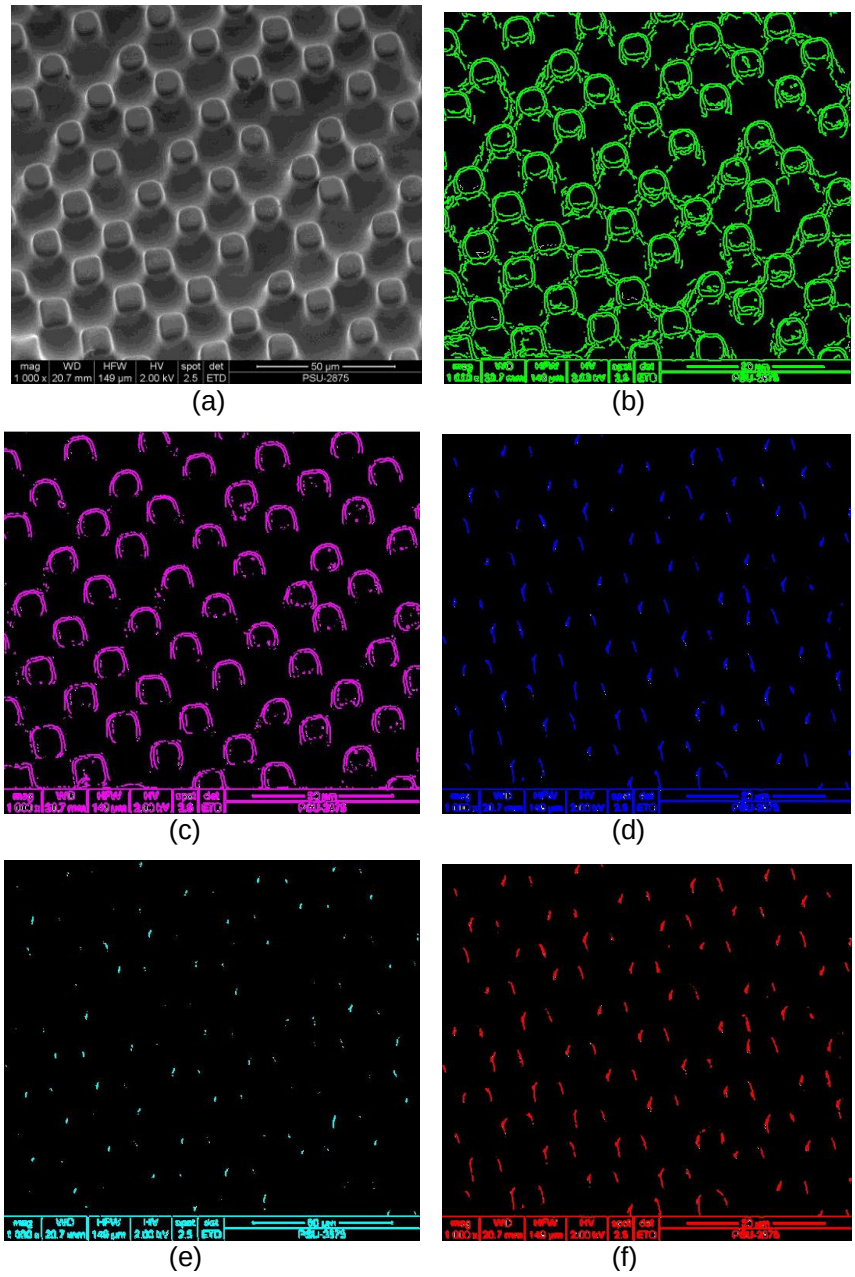

Figure 7. (a) SEM micrograph of SU-8 cross sections and its corresponding outputs from (b) Canny, (c) LoG, (d) Prewitt, (e) Roberts Cross and (f) Sobel operators.

the highest number of 3297 lines indicates substantial false detections by the Canny operator. As a result, the LoG operator stands out as the best candidate for accurate edge detection in the optical microscope image. However, some noise fragments are still present and some edges are missing. The Prewitt and the Sobel operators offer relatively noise-free outputs but at the expense of more missing edges. The effect is more severe when the Roberts Cross edge detection is employed because of its smaller operating matrix. Most missing edges correspond to a low-contrast side of the pillars which is not properly leveled and focused. Failure to detect these edges by the less sensitive operators is unavoidable.

The outputs of an SEM micrograph in Figure 7 clearly divide the algorithms into two groups. The sensitive operators with all pillars detected by more than 1000 lines are the Canny and the LoG operators. As found in the primitive image and the optical micrograph, the drawback of these two algorithms is the noise from spurious

detection in the background. In this case, the bright fringes surround the pillars possibly from the electron charge accumulation that give rise to double edge detections. The low-contrast side of the pillars due to the tilt angle of an electron beam also leads to missing edges in the output from the LoG operator. For the less sensitive operators with under 500 lines detected, the Roberts Cross operator has a weakest response to the edge of micropattern. The detection is only slightly improved by the Prewitt and Sobel operators, but none of the pillars are completely included. This is a proof that the uses of certain edge detectors are limited to 2D images and they are not applicable to SEM micrographs which represent the view from tilt angles.

The performance of the edge detectors under test is application dependent. The Sobel operator may generally be recommended but it is not sensitive enough in the case of low-contrast images which are typical for magnetic micro and nanostructures. The Canny and the LoG operators are more appropriate in such applications due to high sensitivity after the image smoothing and enhancement processes. The spurious detections can be reduced by applying the threshold. Finally, the SEM micrograph in Figure 7 with proper magnification and angle can be used as a sample to quantitatively assess the pattern deviation. An average width of the cross section in this image is 9.64 µm with a standard deviation of 0.46, whereas, the designate spacing between the centers is 20 µm and the real distance is averaged as 18.73 µm with a standard deviation of 2.44.

Conclusions

The array of SU-8 micropillars obtained from the X-ray lithography process exhibits less than 10% deviations in position and geometry from the designate pattern. This patterned substrate can be used for the deposition of cobalt film with small flatness errors. Five image processing algorithms, successfully tested in detecting sharp edges of primitive circles, have different response to the micrographs of patterned pillars. The Canny operator is the most sensitive having all cross sectional pillars detected along with spurious detections. Outputs of the LoG operator also include all pillars with lower noise, but a low-contrast side of the cross sections is not detected. The Prewitt, Sobel and Roberts Cross edge detectors comparatively perform with even less sensitivity to noise and low-contrast edges. As a result, these three operators are not applicable in the case of tilt angled SEM images.

ACKNOWLEDGEMENTS

This work is funded by the Thailand's Synchrotron Light Research Institute (Grant 2552/PS01). A graduate scholarship was granted to U. Phromsuwan by the Industry/University Cooperative Research Center (I/UCRC) in HDD Component, the Faculty of Engineering, Khon Kaen University and National Electronics and Computer Technology Center, National Science and Technology Development Agency. The micrographs were obtained with the assistance of P. Sukonrat and K. Chokprasombat.

REFERENCES

Choi C, Hong D, Oh Y, Noh K, Kim JY, Chen L, Liou SH, Jin S (2010). Enhanced magnetic properties of bit patterned magnetic recording media by trench-filled nanostructure. Elec. Mater. Lett., 6(3): 113-116.

del Campo A, Greiner C (2007). SU-8: a photoresist for high-aspect-ratio and 3D submicron lithography. J. Micromech. Microeng., 17(6): R81-R95.

del Campo A, Arzt E (2008). Fabrication approaches for generating complex micro- and nanopatterns on polymeric surfaces. Chem. Rev., 108(3): 911-945.

Gonzalez RC, Woods RE, Eddins SL (2001). Digital image processing. Pearson Education, New Jersey, pp. 572-585.

Kikitsu A, Kamata Y, Sakurai M, Naito K (2007). Recent progress of patterned media. IEEE Trans. Magn., 43(9): 3685-3688.

Liu QH, Wang HL, Liu J, Huang HY (2011). AFM image processing for estimating the number and volume of nanoparticles on a rough surface. Surf. Interf. Anal., 43(10): 1354-1359.

Marot J, Bourennane S (2007). Subspace-based and DIRECT algorithms for distorted circular contour estimation. IEEE Trans. Image Process., 16(9): 2369-2378.

Moropoulou A, Delegou ET, Vlahakis V, Karaviti E (2007). Digital processing of SEM images for the assessment of evaluation indexes of cleaning interventions on Pentelic marbles surfaces. Mater. Charact., 58(11-12): 1063-1069.

Nabavi S, Vijaya Kumar BVK, Bain JA, Hogg C, Majetich SA (2009). Application of image processing to characterize patterning noise in self-assembled nano-masks for bit-patterned media. IEEE Trans. Magn., 45(10): 3523-3526.

Smereka M, Duleba I (2008). Circular object detection using a modified Hough transform. Int. J. Appl. Math. Comp., 18(1): 85-91.

Sopharak A, Uyyanonvara B, Barman S (2009). Automatic exudate detection for diabetic retinopathy screening. Sci. Asia, 35(1): 80-88.

Terris BD (2009). Fabrication challenge for patterned recording media. J. Magn. Magn. Mater., 321(6): 512-517.

Yakar M, Yilmaz HM, Mutluoglu O (2010). Closed range photogrammy and robotic total station in volume calculation. Int. J. Phys. Sci., 5(2): 86-96.

Zhang S, Xie M, Zhang Y, Wei T (2011). A novel method for object detection based on graph theory. Int. J. Phys. Sci., 6(29): 6735-6740.

Zhao JQ (2010). Simple technique to evaluate effects of nonsphericity and orientation on particle size distribution retrieval. Int. J. Phys. Sci., 6(31): 7100-7105.